[Short title + Author Name - P&H title] 17 (2024) 105933

Contents lists available at ScienceDirect

Arabian Journal of Chemistry

journal homepage: www.ksu.edu.sa

Novel hydroxy-tagged bis-dihydrazothiazole derivatives: Synthesis, antimicrobial capacity and formation of some metal chelates with iron, cobalt and zinc ions

Refaie M. Kassab [a,*], Sami A. Al-Hussain [b], Magdi E.A. Zaki [b], Gehad G. Mohamed [a,c], Zeinab A. Muhammad [d,*]

[a] Chemistry Department, Faculty of Science, Cairo University, Giza 12613, Egypt
[b] Department of Chemistry, Faculty of Science, Imam Mohammad Ibn Saud Islamic University (IMSIU), Riyadh 11623, Saudi Arabia
[c] Nanoscience Department, Basic and Applied Sciences Institute, Egypt-Japan University of Science and Technology, New Borg El Arab, 21934 Alexandria, Egypt
[d] Department of Pharmaceutical Chemistry, National Organization for Drug Control and Research (NODCAR), Giza 12311, Egypt

ARTICLE INFO

Keywords:
Bis-aldehyde thiosemicarbazone
Hydrazonoyl halides
Transition metal complexes
Antibacterial, antifungal prototypes

ABSTRACT

Until today, microbial infections epitomize a serious universal health threat. Subsequently, developing a potential antimicrobial prototype remains an urgent, global necessity. Despite several reports discussing the biological utility of some bis-thiazoles, the use of bis-dihydrazothiazoles and their corresponding metal chelates as potent antimicrobials, is yet to be explored. The current report outlines an attempt to fill that void by representing a successful synthesis of a new class of bis-dihydrazothiazoles as well as three of their transition metal chelates and their use as potential antimicrobials. This report presents the design of some novel hydroxy-tagged bis-dihydrazothiazoles **6a-e** and bis-dihydrazothiazolones **9a-e** *via* the reaction of a bis-aldehyde thiosemicarbazone **3**, as a common synthetic precursor, with two groups of hydrazonoyl halide derivatives **4a-e** and **7a-e**. The chelation affinity of these novel bis-dihydrazothiazoles to behave as neutral tridentate ligands coordinating to the metal ions; Fe(III), Co(II), or Zn(II) through azomethine-*N*, thiazole-*S*, and azo-*N* atoms to form metal complexes with a metal/ligand ratio of 2:1 was confirmed. *In-vitro*, antimicrobial screening of the novel hydroxy-tagged bis-dihydrazothiazole derivatives, as well as a selected group of their transition metal chelate complexes [M_2L], was inspected, and the data were measured in comparison to those of ketoconazole and gentamycin as antimicrobial reference standards. Most bis-dihydrazothiazoles **6a-e** and bis-dihydrazothiazolones **9a-e** showed decent to excellent antimicrobial activities against the screened microbes, but the chloro-substituted bis dihydrazothiazole derivatives **6c** and **9c** showed exceptional inhibition of *Bacillus subtilis* (20 mm), *Escherichia coli* (25 mm), and *Candida albicans* (19 mm), and *Salmonella typhimurium* (19 mm), respectively. Additionally, amongst the three synthesized metal complexes **[M_2L]**, only the zinc complex, **[Zn_2L]** showed remarkable inhibition of both *Staphylococcus aureus* (21 mm) *and Salmonella typhimurium* (19 mm) compared to the reference standard *Gentamycin*, and was more potent than the free ligand, **6a** itself (no activity and 11 mm respectively). Antimicrobial inspection was assessed by the agar well diffusion assay method against all bacterial and fungal strains. Magnetic moment, diffused reflectance, FT-IR, ^{1}H NMR, molar conductivity, thermogravimetric analysis (TGA), X-ray diffraction (XRD), and scanning electron microscope (SEM) were among the many techniques used to elucidate the structures of all novel hydroxy-tagged bis-heterocyclic ligands and their metal chelate complexes.

1. Introduction

The thiazole ring has been one of the more interesting heterocycles amongst the synthetic and pharmaceutical communities (Potewar et al., 2007; Rajanarendar et al., 2012; Petrou et al., 2021). The wide spectrum of its pharmacological applications makes the thiazole ring an attractive pharmacophore nucleus. The thiazole nucleus presents the pharmacophoric center in various biologically active compounds (Potewar et al.,

* Corresponding authors.
E-mail addresses: rkassab@sci.cu.edu.eg (R.M. Kassab), Mezaki@imamu.edu.sa (M.E.A. Zaki), zeinab.a.muhammad@gmail.com (Z.A. Muhammad).

https://doi.org/10.1016/j.arabjc.2024.105933
Received 18 March 2024; Accepted 22 July 2024
Available online 23 July 2024

2007; Rajanarendar et al., 2012; Petrou et al., 2021; Abdelhamid et al., 2015; Dawood and Gomha, 2015; Gomha et al., 2015; Sayed et al., 2020; Abdel-Wahab et al., 2008; Verma and Saraf, 2008). Several thiazole derivatives are well-known biologically active scaffolds (Petrou et al., 2021; Verma and Saraf, 2008), which make them outstanding nominees for structural-based pharmacological screening (Oka et al., 2012; Watanabe and Uesugi, 2013).

Many thiazole derivatives span a wide range of pharmacological activities such as antifungal (Zhang et al., 2023); antimicrobial (Limban et al., 2008); antibacterial (Kassab et al., 2022); anti-inflammatory (Franklin et al., 2008; Kouatly et al., 2009); analgesic (Yücel et al., 2024); antihypertensive (Abdel-Wahab et al., 2008); anti-HIV agents (Israr et al., 2024); or anticancer (Rana et al., 2023). Additionally, the thiazole nucleus was incorporated into numerous clinically approved antimicrobial drugs (Fig. 1) (Niu et al., 2023).

Similar to their parent thiazole analogs, numerous bis-thiazole derivatives were found to be biologically active as antimicrobial (Kassab et al., 2021; Borcea et al., 2021); antifungal (Clough et al., 2006); antiviral (Kassab et al., 2024); antibiotics (Cascioferro et al., 2020); or anticancer (Rana et al., 2023). Moreover, the ability of many organic molecules in general and bis-heterocycles, *aka*, bidentate and tridentate ligands in particular, to coordinate with metal ions forming metal complexes make them very attractive targets for various, including medicinal, applications (Karges et al., 2021). As a result, several recent reports have discussed the rich biological diversity of several transition metal ion complexes, especially with azo-containing ligands (Kyhoiesh and Hassan, 2024; Kyhoiesh and Al-Adilee, 2023; Kyhoiesh and Al-Adilee, 2022). However, up to the present moment, microbial infections represent a serious global health threat. Subsequently, developing new antimicrobial drug prototypes remains an urgent, universal necessity. Despite several reports discussing the biological functionality of some bis-thiazoles (Kassab et al., 2021; Borcea et al., 2021; Clough et al., 2006; Kassab et al., 2024); the use of bis-dihydrazothiazole and their corresponding transition metal chelates as potential antimicrobials, is yet to be investigated.

Considering these verdicts, and in extension of our everlasting conquest in the construction of heterocyclic (Kassab et al., 2023; Al-Hussain et al., 2024; Kassab et al., 2024) and bis-heterocyclic compounds (Kassab et al., 2016; Sanad et al., 2016; Mahmoud et al., 2019; Kassab et al., 2020; Kassab et al., 2022; Kassab et al., 2022; Kassab et al., 2023); we dedicated the current study to build some novel hydroxy-tagged bis-dihydrazothiazole derivatives with prominent biological capacity. In this account, the construction protocol of some hydroxy-tagged bis-dihydrazothiazoles and bis-dihydrazothiazolone derivatives was outlined using a hydroxy-tagged bis-thiosemicarbazone derivative **3** as a common synthetic scaffold. The hydroxyl group was incorporated to serve the purpose of future fine-tuning of the structural activity relationship (SAR) via several possible synthetic modifications (Ou et al., 2013).

Additionally, the preliminary coordination characteristics of these novel hydroxy-tagged bis-dihydrazothiazole derivatives were probed by studying their interactions with Fe(III), Cr(II), and Zn(II) transition metal ions. Furthermore, the antimicrobial behavior of these novel hydroxy-tagged bis-dihydrazothiazole derivatives as well a selected group of their metal chelates with some transition metals was examined via *in-vitro* screening. The antimicrobial activity data were measured in comparison to those of *ketoconazole* and *gentamycin* as antimicrobial standards.

2. Experimental

2.1. Chemicals and instruments

The chemicals, and reagents (analytical grade) used in the research were acquired from Float chemicals and reagents, BDH laboratory chemicals, and Sigma-Aldrich. They include 4-sbstituted anilines (99 %), 4-hydroxybenzaldehyde (99 %), epichlorohydrin (99 %), thiosemicarbazide (98 %), $Co(OCOCH_3)_2{\cdot}4H_2O$ (99 %), $Fe(NO_3)_3{\cdot}9H_2O$ (99 %), and $Zn(OCOCH_3)_2{\cdot}4H_2O$ (99 %). Melting points of the ligands and complexes were determined by using a Gallen Kamp apparatus. The carbon, hydrogen, and nitrogen content of the solid complexes was determined using a CHNS-932 (LECO) Vario elemental analyzer. The Fourier transform infrared (FT-IR) spectra were recorded using a Perkin Elmer 1650 spectrophotometer with potassium bromide (KBr) pellets as the sample matrix. The range of analysis was 400–4000 cm^{-1}. Molar magnetic susceptibility was measured on powdered samples using the Faraday method. Diamagnetic corrections were made using Pascal's constant and $Hg[Co(SCN)_4]$ was used as a calibrant. Molar conductivities of 10^{-3} M solutions of the solid complexes in ethanol were measured using a Jenway 4010 conductivity meter. The ^1H NMR spectra were recorded on a 300 MHz Varian-Oxford Mercury spectrometer at room temperature as solutions in DMSO-d_6, with tetramethyl silane as an internal standard. Chemical shifts are expressed as parts per million (ppm) to TMS. The mass spectra were recorded using a Hewlett-Packard MS-5988 GS-MS apparatus with the electron ionization method at 70 eV. 1×10^{-3} M solutions of the solid complexes in dimethylformamide (DMF) were used to measure the molar conductivities using a Jenway 4010 conductivity meter. Thermogravimetric (TG) and differential thermogravimetric (DTG) analysis of the solid complexes were carried out at

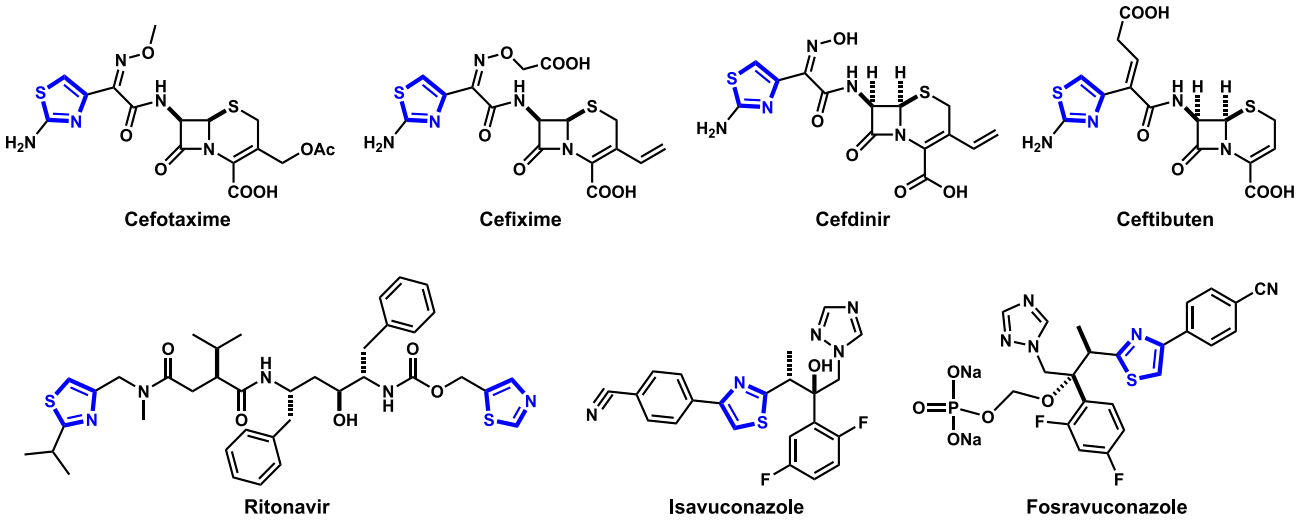

Fig. 1. Some thiazole-containing clinically used antimicrobial drugs.

ambient temperature and up to 800 °C using a Shimadzu TG-50H thermal analyzer. At the Cairo University, Faculty of Nanotechnology, X-ray diffractions (XRDs) were measured using a Bruker D8 Discover (Bruker AXS Inc., 35 KV, 30 mA) X-ray diffractometer with a step size of 0.02 and a speed scan of 0.016. The Cu Kα radiation (λ = 1.5406 Å) was used for the measurement for two hours, with 2θ ranging from 5 to 80. A Japanese Jol 2000 scanning electron microscope (SEM) was used to take pictures of all transition metal complexes. Under measuring conditions (size 500 X 500 nm, contact mode, speed 0.5 in./sec), the suspension was placed to a mica slide.

2.1.1. Synthesis of bis-thiosemicarbazone derivative 3

Bis-thiosemicarbazone derivative **3** was prepared using a modified reported procedure by our research group (Kassab et al., 2021; Kassab et al., 2022). To an ethanolic (30 ml) mixture of hydroxy-bis-aldehyde **1** (3.00 g, 0.01 mol) containing a few drops of conc. HCl, thiosemicarbazide (4.46 g, 0.01 mol) was added and the mixture was refluxed for 3 h. The formed ppt upon cooling was collected and recrystallized from a mixture of ethanol/dioxane 3:1 (v/v) as yellow crystals,72 % yield; mp > 300 °C; IR: 3471, 3350 (NH_2), 3185 (NH), 1510 (C=N) cm^{-1}; ^{1}H NMR: δ 2.50 (br, 1H, OH), 4.1–4.3 (m, 5H, OCH_2, OCH), 6.90–8.00 (m, 12H, ArH, NH_2), 8.15 (s, 2H, CH=N), 11.25 (s, 2H, NH); MS *m/z* (%): 446 (M^+, 57), 450 (69), 432 (57), 380 (44), 346 (53), 232 (47), 218 (38), 195 (82), 135 (100), 121 (80), 99 (58). Anal. Calcd for $C_{19}H_{22}N_6O_3S_2$ (446.54 g/mol): C, 51.11; H, 4.97; N, 18.82. Found: C, 51.0; H, 4.79; N, 18.75.

2.2. General procedure for the synthesis of bis-dihydrazothiazole derivatives **6a-e, 9a-e**

To a stirred solution of thiosemicarbazone derivative **3** (1.1 g, 2.5 mmol) and tow equivalent of hydrazonoyl chloride derivative **4a-e, 7a-e (**5 mmol) in dioxane (30 mL), was added triethylamine (0.7 mL) and the mixture was refluxed for 5 h. The precipitated triethylamine hydrochloride was filtered off, and the solvent of the filtrate was subjected to evaporation under reduced pressure. The residue was triturated with methanol. The formed solid was collected by filtration, washed with water, dried, and recrystallized from dioxane to afford the corresponding *bis*-thiazole derivatives **6a-e**, **9a-e** respectively.

2.2.1. 1,3-Bis(4-((2-(4-methyl-5-(phenyldiazenyl)thiazol-2-yl)hydrazono) methyl)phenoxy)propan-2-ol (6a)

Following the general procedure, thiosemicarbazone derivative **3** (1.1 g, 2.5 mmol) and hydrazonoyl chloride derivative **4a** (0.98 g, 5 mmol) gave compound **6a** as red solid, 74 % yield; mp 240–241 °C; IR: *ν* 3430 (2NH), 3030, 2930 (C–H) cm^{-1}; ^{1}H- NMR δ 2.43 (s, 6H, $2CH_3$), 4.16–4.21 (m, 5H, OCH_2, OCH), 5.53 (s, 1H, OH), 6.98–8.00 (m, 18H, Ar-H), 8.56 (s, 2H, 2CH=N), 10.50 (s, 2H, 2NH) ppm; MS *m/z* (%): 730 (M^+, 57), 711 (46), 692 (30), 613 (28), 585 (45), 565 (45), 459 (69), 421 (57), 381 (44), 357 (53), 235 (43), 218 (38), 197 (44), 137 (100), 123 (80), 99 (58). Anal. Calcd for $C_{37}H_{34}N_{10}O_3S_2$ (730.87 g/mol): C, 60.81; H, 4.69; N, 19.16. Found: C, 60.53; H, 4.40; N, 18.85.

2.2.2. 1,3-Bis(4-((2-(4-methyl-5-(p-tolyldiazenyl)thiazol-2-yl)hydrazono) methyl)phenoxy)propan-2-ol (6b)

Following the general procedure, thiosemicarbazone derivative **3** (1.1 g, 2.5 mmol) and hydrazonoyl chloride derivative **4b** (1.05 g, 5 mmol) gave compound **6b** as red solid, 71 % yield; mp 204–205 °C; IR: *ν* 3425 (2NH), 3014, 2920 (C–H) cm^{-1}; ^{1}H NMR: δ 2.24 (s, 6H, $2CH_3$), 2.49 (s, 6H, $2CH_3$), 4.11–4.21 (m, 5H, OCH_2, OCH), 5.50 (s, 1H, OH), 7.09–7.81 (m, 16H, Ar-H), 8.54 (s, 2H, 2CH=N), 10.54 (s, 2H, 2NH) ppm; ^{13}C NMR: δ 21.1, 24.3 ($4CH_3$), 26.3 (2CH), 52.3 ($2CH_2$), 115.1, 115.6, 124.4, 126.7, 128.2, 128.4, 128.5 129.5, 130.9, 136.5, 140.4, 152.7, 160.3 (Ar-H and C=N) ppm; MS *m/z* (%): 759 (M^+, 26), 755 (35), 725 (43), 691 (22), 619 (30), 568 (25), 526 (100), 506 (38), 483 (35), 391 (26), 353 (36), 266 (52), 249 (60), 92 (42), 62 (43). Anal. Calcd. for $C_{39}H_{38}N_{10}O_3S_2$ (758.92 g/mol): C, 61.72; H, 5.05; N, 18.46. Found: C, 61.50; H, 4.78; N, 18.28.

2.2.3. 1,3-Bis(4-((2-(5-((4-chlorophenyl)diazenyl)-4-methylthiazol-2-yl) hydrazono)methyl) phenoxy)propan-2-ol (6c)

Following the general procedure, thiosemicarbazone derivative **3** (1.1 g, 2.5 mmol) and hydrazonoyl chloride derivative **4c** (1.15 g, 5 mmol) gave compound **6c** as red solid, 75 % yield; mp 199–200 °C; IR: *ν* 3402 (2NH), 3098, 2931 (C–H) cm^{-1}; ^{1}H NMR: δ 2.43 (s, 6H, $2CH_3$), 4.16–4.21 (m, 5H, OCH_2, OCH), 5.54 (s, 1H, OH), 6.98–8.00 (m, 16H, Ar-H), 8.55 (s, 2H, 2CH=N), 10.35 (s, 2H, 2NH) ppm; MS *m/z* (%): 799 (M^+, 9), 777 (35), 760 (16), 670 (17), 622 (23), 588 (16), 550 (24), 535 (26), 480 (45), 449 (61), 426 (47), 383 (38), 301 (68), 299 (96), 254 (86), 223 (66), 163 (43), 150 (100), 120 (98), 93 (47). Anal. Calcd. for $C_{37}H_{32}Cl_2N_{10}O_3S_2$ (799.75 g/mol): C, 55.57; H, 4.03; N, 17.51. Found: C, 55.35; H, 3.75; N, 17.25.

2.2.4. 1,3-Bis(4-((2-(5-((4-bromophenyl)diazenyl)-4-methylthiazol-2-yl) hydrazono)methyl) phenoxy)propan-2-ol (6d)

Following the general procedure, thiosemicarbazone derivative **3** (1.1 g, 2.5 mmol) and hydrazonoyl chloride derivative **4d** (1.37 g, 5 mmol) gave compound **6d** as red solid, 76 % yield; mp 224–225 °C; IR: *ν* 3433 (2NH), 3065, 2929 (CH) cm^{-1}; ^{1}H- NMR: δ 2.43 (s, 6H, $2CH_3$), 4.17–4.21 (m, 5H, OCH_2, OCH), 5.40 (s, 1H, OH), 7.10–7.82 (m, 16H, Ar-H), 8.55 (s, 2H, 2CH=N), 10.25 (s, 2H, 2NH) MS *m/z* (%): 888 (M^+, 21), 870 (33), 841 (44), 824 (94), 774 (42), 761 (38), 702 (50), 667 (67), 632 (63), 606 (51), 542 (42), 501 (48), 447 (41), 405 (57), 366 (74), 301 (45), 280 (91), 201 (100), 151 (95). Anal. Calcd. for $C_{37}H_{32}Br_2N_{10}O_3S_2$ (888.66 g/mol): C, 50.01; H, 3.63; N, 15.76. Found: C, 50.45; H, 3.45; N, 15.55.

2.2.5. 1,3-Bis(4-((2-(5-((4-fluorophenyl)diazenyl)-4-methylthiazol-2-yl) hydrazono)methyl) phenoxy)propan-2-ol (6e)

Following the general procedure, thiosemicarbazone derivative **3** (1.1 g, 2.5 mmol) and hydrazonoyl chloride derivative **4e** (1.07 g, 5 mmol) gave compound **6e** as red solid, 78 % yield; mp 209–210 °C; IR: *ν* 3448 (2NH), 2988, 2935 (CH) cm^{-1}; ^{1}H NMR: δ 2.48 (s, 6H, $2CH_3$), 4.16–4.21 (m, 5H, OCH_2, OCH), 5.62 (s, 1H, OH), 7.09–7.82 (m, 16H, Ar-H), 8.55 (s, 2H, 2CH=N), 10.50 (s, 2H, 2NH) ppm; ^{13}C NMR: δ 25.8 ($2CH_3$), 43.2, 63.2, 67.5 ($2CH_2$, CH-OH), 113.5, 115.3, 119.2, 127.8, 129.1, 131.6, 133.5, 134.6, 144.4, 146.5, 158.3 (Ar-H and C=N) ppm; MS *m/z* (%): 766 (M^+, 15), 742 (12), 710 (15), 667 (21), 657 (24), 610 (11), 568 (16), 566 (20), 524 (13), 466 (28), 386 (10), 285 (21), 238 (53), 201 (100), 135 (34), 94 (22). Anal. Calcd. for $C_{37}H_{32}F_2N_{10}O_3S_2$ (766.85 g/mol): C, 57.95; H, 4.21; N, 18.27. Found: C, 58.20; H, 3.95; N, 18.15.

2.2.6. 2,2′-(((((2-Hydroxypropane-1,3-diyl)bis(oxy))bis(4,1-phenylene)) bis(methanylylidene))bis (hydrazin-1-yl-2-ylidene))bis(5-(2-phenylhydrazono)thiazol-4(5H)-one) (9a)

Following the general procedure, thiosemicarbazone derivative **3** (1.1 g, 2.5 mmol) and hydrazonoyl chloride derivative **7a** (1.13 g, 5 mmol) gave compound **9a** as yellow solid, 71 % yield; mp 158–159 °C; IR: *ν* 3390, 3280 (4NH), 3073, 3015, 2975 (CH), 1720 (2C=O) cm^{-1}; ^{1}H NMR: δ 4.12–4.40 (m, 5H, OCH_2, OCH), 5.48 (s, 1H, OH), 6.86–7.91 (m, 18H, Ar-H), 8.38 (s, 2H, 2CH=N), 10.78 (s, 2H, 2NH), 11.21 (s, 2H, 2NH) ppm; MS *m/z* (%): 734 (M^+, 24), 709 (34), 682 (55), 634 (30), 595 (33), 430 (44), 319 (39), 309 (100), 236 (46), 200 (30), 159 (38), 151 (46), 131 (34), 59 (74), 54 (50). Anal. Calcd. for $C_{35}H_{30}N_{10}O_5S_2$ (734.81 g/mol): C, 57.21; H, 4.12; N, 19.06. Found: C, 57.00; H, 3.94; N, 18.88.

2.2.7. 2,2′-(((((2-Hydroxypropane-1,3-diyl)bis(oxy))bis(4,1-phenylene)) bis(methanylylidene))bis (hydrazin-1-yl-2-ylidene))bis(5-(2-(p-tolyl) hydrazono)thiazol-4(5H)-one) (9b)

Following the general procedure, thiosemicarbazone derivative **3** (1.1 g, 2.5 mmol) and hydrazonoyl chloride derivative **7b** (1.2 g, 5

mmol) gave compound **9b** as yellow solid, 73 % yield; mp 168–169 °C; IR: *ν* 3441, 3275 (4NH), 3073, 2931 (CH), 1728 (2C=O) cm^{-1}; ^1H NMR: *δ* 1.90 (s, 6H, $2CH_3$), 4.13–4.34 (m, 5H, OCH_2, OCH), 5.47 (s, 1H, OH), 6.87–7.99 (m, 16H, Ar-H), 8.45 (s, 2H, 2CH=N), 10.49 (s, 2H, 2NH), 11.29 (s, 2H, 2NH) ppm; ^{13}C NMR: *δ* 14.8 ($2CH_3$), 28.9 (CH-OH), 32.1 ($2CH_2$), 65.6, 89.4, 113.5, 116.6, 118.5, 121.0, 123.7, 125.5, 128.2, 129.9, 130.8 (Ar-H and C=N), 158.0 (2C=O) ppm; MS *m/z* (%): 762 (M^+, 15), 758 (24), 662 (19), 560 (28), 516 (71), 506 (74), 481 (38), 448 (50), 433 (81), 414 (86), 377 (86), 343 (100), 109 (53), 53 (72), 43 (68). Anal. Calcd. for $C_{37}H_{34}N_{10}O_5S_2$ (762.86 g/mol): C, 58.26; H, 4.49; N, 18.36. Found: C, 58.55; H, 4.24; N, 18.14.

2.2.8. 2,2′-(((((2-Hydroxypropane-1,3-diyl)bis(oxy))bis(4,1-phenylene))bis(methanylylidene))bis (hydrazin-1-yl-2-ylidene))bis(5-(2-(4-chloro phenyl)hydrazono)thiazol-4(5H)-one) (9c)

Following the general procedure, thiosemicarbazone derivative **3** (1.1 g, 2.5 mmol) and hydrazonoyl chloride derivative **7c** (1.3 g, 5 mmol) gave compound **9c** as yellow solid, 74 % yield; mp 165–166 °C; IR: *ν* 3430, 3250 (4NH), 3150, 2968 (CH), 1729 (C=O) cm^{-1}; ^1H NMR: *δ* 4.09–4.32 (m, 5H, OCH_2, OCH), 5.42 (s, 1H, OH), 6.87–7.89 (m, 16H, Ar-H), 8.45 (s, 2H, 2CH=N), 10.49 (s, 2H, 2NH), 11.28 (s, 2H, 2NH) ppm; ^{13}C NMR: *δ* 28.9 (CH-OH), 32.9 (2CH2), 61.0, 115.5, 116.6, 120.8, 127.5, 129.3, 133.3, 138.0, 142.1, 143.1, 152.0 (Ar-H and C=N), 162.6 (2C=O) ppm; MS *m/z* (%): 803 (M^+, 6), 798 (10), 760 (10), 686 (33), 550 (42), 504 (31), 463 (38), 431 (81), 368 (79), 354 (34), 323 (34), 255 (52), 236 (100), 139 (32), 114 (38), 96 (41), 59 (40). Anal. Calcd. for $C_{35}H_{28}Cl_2N_{10}O_5S_2$ (803.69 g/mol): C, 52.31; H, 3.51; N, 17.43. Found: C, 52.55; H, 3.30; N, 17.16.

2.2.9. 2,2′-(((((2-hydroxypropane-1,3-diyl)bis(oxy))bis(4,1-phenylene))bis(methanylylidene))bis (hydrazin-1-yl-2-ylidene))bis(5-(2-(4-bromo phenyl)hydrazono)thiazol-4(5H)-one) (9d)

Following the general procedure, thiosemicarbazone derivative **3** (1.1 g, 2.5 mmol) and hydrazonoyl chloride derivative **7d** (1.5 g, 5 mmol) gave compound **9d** as yellow solid, 70 % yield; mp 160–162 °C; IR (KBr):*ν* 3441, 3200 (4NH), 2978, 2947 (C–H), 1726 (C=O) cm^{-1}; ^1H NMR: *δ* 4.14–4.19 (m, 5H, OCH_2, OCH), 5.33 (s, 1H, OH), 7.08–7.88 (m, 16H, Ar-H), 8.45 (s, 2H, 2CH=N), 10.49 (s, 2H, 2NH), 11.22 (s, 2H, 2NH) ppm; MS *m/z* (%): 892 (M^+, 60), 737 (35), 707 (25), 650 (29), 551 (48), 513 (30), 474 (61), 388 (31), 341 (35), 268 (30), 214 (32), 199 (23), 75 (88), 57 (100). Anal. Calcd for $C_{35}H_{28}N_{12}O_9S_2$ (892.60 g/mol): C, 47.10; H, 3.16; N, 15.69. Found: C, 47.32; H, 3.35; N, 15.51.

2.2.10. 2,2′-(((((2-Hydroxypropane-1,3-diyl)bis(oxy))bis(4,1-phenylene))bis(methanylylidene))bis (hydrazin-1-yl-2-ylidene))bis(5-(2-(4-fluorophenyl)hydrazono)thiazol-4(5H)-one) (9e)

Following the general procedure, thiosemicarbazone derivative **3** (1.1 g, 2.5 mmol) and hydrazonoyl chloride derivative **7e** (1.22 g, 5 mmol) gave compound **9e** as yellow solid, 73 % yield; mp 172–173 °C; IR (KBr): *ν* 3415, 31,522 (4NH), 3154, 2970 (CH), 1728 (2C=O) cm^{-1}; ^1H NMR: *δ* 4.06–4.39 (m, 5H, OCH_2, OCH), 5.46 (s, 1H, OH), 6.87–7.89 (m, 16H, Ar-H), 8.61 (s, 2H, 2CH=N), 11.22 (s, 2H, 2NH) ppm; ^{13}C NMR: *δ* 27.5 (CH-OH), 30.0 ($2CH_2$), 65.3, 112.7, 114.1, 116.7, 120.8, 128.6, 129.9, 131.8, 132.3, 139.5, 143.5 (Ar-H and C=N), 171.3 (2C=O) ppm; MS *m/z* (%): 770 (M^+, 12), 710 (10), 665 (20), 640 (90), 585 (24), 501 (57), 467 (16), 320 (26), 255 (38), 160 (43), 148 (81), 117 (100), 90 (68). Anal. Calcd. For $C_{35}H_{28}F_4N_{10}O_5S_2$ (770.79 g/mol): C, 54.54; H, 3.66; N, 18.17. Found: C, 54.76; H, 3.52; N, 18.00.

2.3. General procedure for the synthesis of bis-dihydrazothiazole metal chelates M_2L, M=Fe(III), Co(II), and Zn(II); L=bis-dihydrazothiazole derivative 6a

A DMF/ethanol 3:1 (v/v) solution of the synthesized bis-dihydrazothiazole ligand **6a** (400 mg, 0.548 mmol) was mixed dropwise with an ethanolic salt solution of ferric nitrate nonahydrate (430 mg, 1.096 mmol), cobalt acetate tetrahydrate (273 mg, 1.096 mmol), or zinc acetate tetrahydrate (241 mg, 1.096 mmol). The mixture was refluxed for 4 h. The solid formed upon cooling was filtered off, washed with ethanol, and vacuum dried.

2.3.1. $[Fe_2(L)(NO_3)_6]$

1,3-*Bis*(4-((2-(4-methyl-5-(phenyldiazenyl)thiazol-2-yl)hydrazono) methyl)phenoxy)propan-2-ol bis(ferric(III) trinitrate). Yield 84 %; mp > 300 °C; Brown solid. Anal. Calc. for $C_{37}H_{34}N_{16}O_{21}S_2Fe_2$ (%): C, 36.55; H, 2.80; N, 18.44; S, 5.27; Fe, 9.22. Actual (%): C, 36.51; H, 2.78; N, 18.27; S, 4.98; Fe, 8.93. Λ_m ($\Omega^{-1}mol^{-1}cm^2$) = 16; FT-IR (*ν*, cm^{-1}): thiazole-N ring (C=N) 1680 s, azomethine (C=N) 1636sh, N=N azo 1470 m, thiazole-S ring (C-S) 1050 s, 741 s, (M−O) 510w, (M−N) 470w, (M−S) 430w. μ_{eff} (BM): 5.66.

2.3.2. $[Co_2(L)(H_2O)_4(AcO)_2].2AcO{\cdot}2H_2O$

1,3-*Bis*(4-((2-(4-methyl-5-(phenyldiazenyl)thiazol-2-yl)hydrazono) methyl)phenox**y**)propan-2-ol bis(cobalt(II) acetate-diaquo)diaceta tedihydrate. Yield 90 %; mp > 300 °C; Brown solid. Anal. Calc. for $C_{37}H_{58}N_{10}O_{17}S_2Co_2$ (%): C, 45.27; H, 4.86; N, 11.74; S, 5.37; Co, 9.89. Actual (%): C, 45.28; H, 4.80; N, 11.58; S, 5.18; Co, 9.73. Λ_m ($\Omega^{-1}mol^{-1}cm^2$) = 96; FT-IR (*ν*, cm^{-1}): thiazole-N ring (C=N) 1659sh, azomethine (C=N) disappeared, N=N azo 1450 s, coordinated water stretching 875w, 850 s, thiazole-S ring (C-S) 1026 m, 750 s, (M−O) 575 s, (M−N) 500 s, (M−S) 450w. μ_{eff} (BM): 4.61.

2.3.3. $[Zn_2(L)(H_2O)_4(AcO)_2].2AcO{\cdot}2H_2O$

1,3-*Bis*(4-((2-(4-methyl-5-(phenyldiazenyl)thiazol-2-yl)hydrazono) methyl)phenoxy)propan-2-ol bis(zinc(II) acetate-diaquo)diacetatedi hydrate. Yield 85 %; mp > 300 °C; Brown solid. Anal. Calc. for $C_{37}H_{58}N_{10}O_{17}S_2Zn_2$ (%): C, 44.82; H, 4.81; N, 11.62; S, 5.31; Zn, 10.79. Actual (%): C, 44.68; H, 4.80; N, 11.48; S, 5.11; Cd, 10.58. Λ_m ($\Omega^{-1}mol^{-1}cm^2$) = 99. FT-IR (*ν*, cm^{-1}): thiazole-N ring (C=N) 1650 s, azomethine (C=N) 1630sh, N=N azo 1475 s, coordinated water stretching 880w, 825 s, thiazole-S ring (C-S) 1026 m, 756 m, (M−O) 575w, (M−N) 480 s, (M−S) 430w. μ_{eff} (BM): diamagnetic. ^1H- NMR *δ* 2.49 (s, 6H, $2CH_3$), 4.14–4.40 (m, 5H, OCH_2, OCH), 5.55 (s, 1H, OH), 6.99–7.94 (m, 18H, Ar-H), 8.61 (s, 2H, 2CH=N), 9.84 (s, 2H, 2NH) ppm.

2.4. Method of antimicrobial screening

The Agar well diffusion method was used to evaluate the antimicrobial activity of the newly synthesized bis-dihydrazothiazole derivatives **6a-e** and **9a-e** along with a few metal complexes of **6a** as a free ligand and a representative example of these new bis-heterocyclic compounds. The surface of the agar plate is inoculated by spreading a volume of the microbial inoculum over the entire agar surface. Then, using a sterile cork-borer or a tip, a 6 mm diameter hole is punched aseptically, and a specific volume (50 μl) of the antimicrobial agent or extract solution at the desired concentration is introduced into the well. The agar plates are then incubated under suitable conditions depending on the test microorganism. The antimicrobial agent diffuses into the agar medium and inhibits the growth of the test microbial strain (Magaldi et al., 2004).DMSO was used as negative control, while ketoconazole and gentamycin were used positive controls.

3. Results and discussion

3.1. Synthesis of Hydroxy-Tagged Bis-Dihydrazothiazole derivatives

To initiate our synthetic approach, the parent bis-thiosemicarbazone derivative **3** was obtained by condensing two equivalents of thiosemicarbazide **(2)** with one equivalent of hydroxy-bearing bis-aldehyde **1** in boiling ethanol, in the presence of a catalytic amount of HCl, for two hours as shown in scheme 1. Bis-aldehyde **1** was prepared analogously to the method reported by Bin *et al.* (Zhao et al., 1996), by heating two

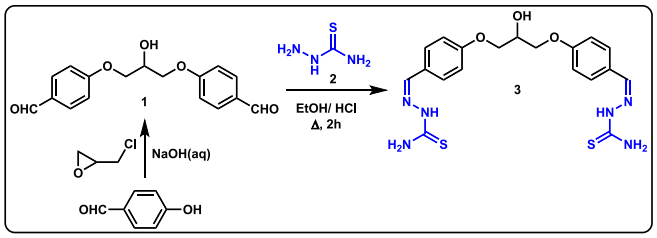

Scheme 1. Synthesis of bis-thiosemicarbazone **3.**

equivalents of salicylaldehyde with one equivalent of epichlorohydrin in an aqueous solution of NaOH (Scheme 1).

To create a novel set of bis-thiazoles, the chemical reactivity of the new hydroxy-bearing bis-thiosemicarbazone **3** towards a variety of hydrazonoyl chlorides **4** was investigated. As a result, the reaction of bis-thiosemicarbazone **3** with hydrazonoyl chlorides **4a-g** in boiling dioxane with catalytic triethylamine yielded the desired bis-thiazoles **6a-g**, presumably through intermediate **5a-g**, as outlined in Scheme 2. Several spectral techniques were used to confirm the structures of all novel bis-thiazole derivatives. The IR spectrum of compound **6a**, for example, showed a typical –NH absorption at ν 3430 cm^{-1}. Furthermore, the ^1H NMR spectrum of **6a** revealed four typical singlets for the $\underline{CH_3}$, CH-$\underline{OH}$, $\underline{CH}$=N, and $\underline{NH}$ groups at 2.43, 5.53, 8.56, and 10.50 ppm, respectively. The distinctive multiplet for the two CH_2 groups, as well as the C–H multiplet, may be seen at 4.16–4.21 ppm.

Under analogous reaction conditions, boiling dioxane and catalytic triethylamine, the parent hydroxy-tagged bis-thiosemicarbazone derivative **3** interacted with *N*-aryl-2-oxopropanehydrazonoyl halides **7a-e** (the ester equivalents of compounds **4a-e**) to create the desired bis-thiazole derivatives **9a-e**, presumably through intermediates **8a-g** as shown in scheme 3. The formation of the new bis-heterocycles **9a-e** was supported by extensive spectral investigations. The IR spectrum of derivative **9b**, for example, revealed the characteristic –NH absorption at 3441 and 3275 cm^{-1}, which is characteristic of the two –NH groups. The isolated bis-thiazole derivatives **9a-e** were structurally confirmed using their ^1H NMR spectra, which had four singlets for the CH-$\underline{OH}$, $\underline{CH}$=N, and $\underline{2NH}$ protons near 5.47, 8.45, 10.49, and 11.29 ppm, respectively.

3.2. Synthesis and characterization of bis-dihydrazothiazole metal chelates

*3.2.1. Synthesis of bis-dihydrazothiazole metal chelates M_2L, M=Fe(III), Co(II), and Zn(II); L=bis-dihydrazothiazole derivative **6a***

The chelating potential of the novel hydroxy-tagged bis-dihydrazothiazole derivative **6a** was studied as an example of all the synthesized bis thiazole ligand as they all have the same coordination sites. Iron(III), cobalt(II), and zinc(II) metal ions were used to synthesize the corresponding metal chelates as an example of trivalent (Fe(III)),

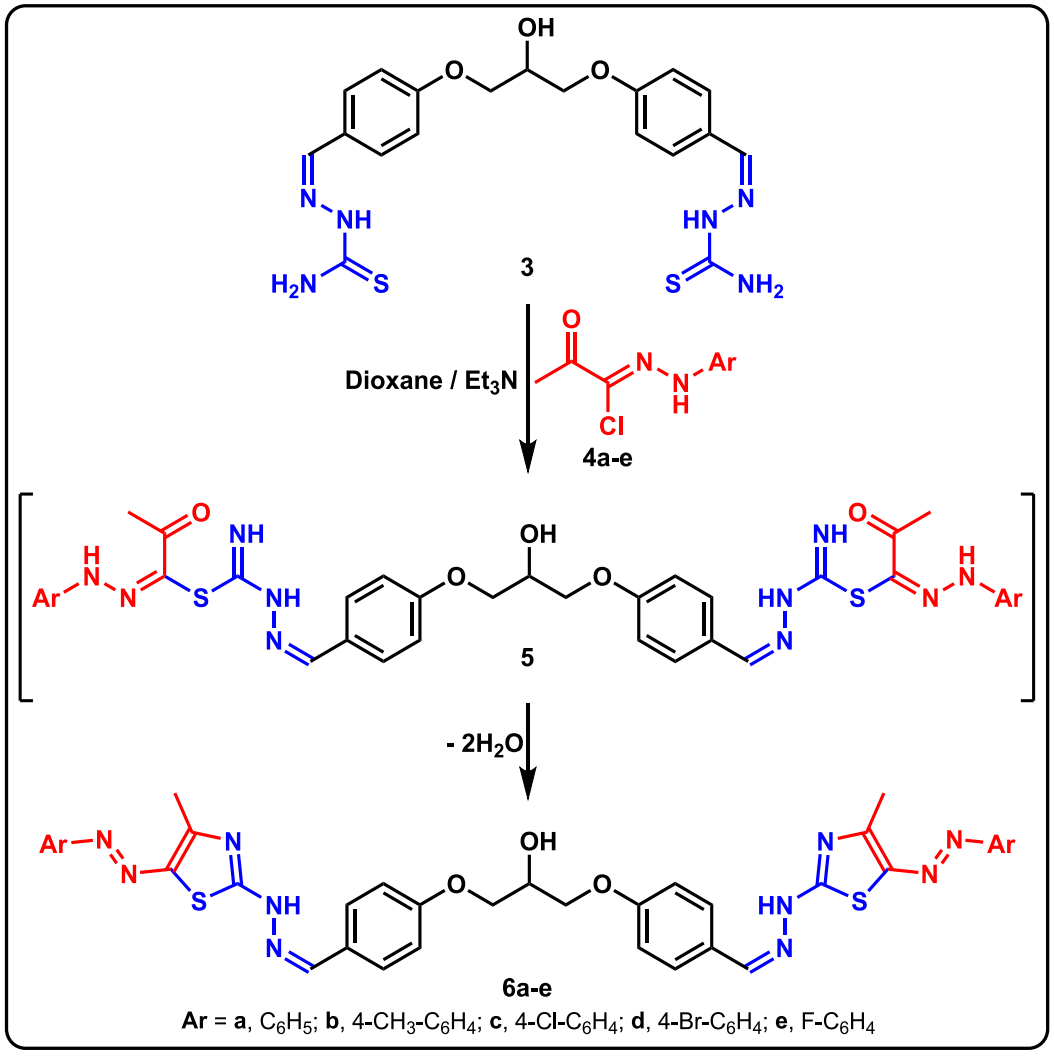

Scheme 2. Synthesis of bis-thiazole derivatives **6a-e.**

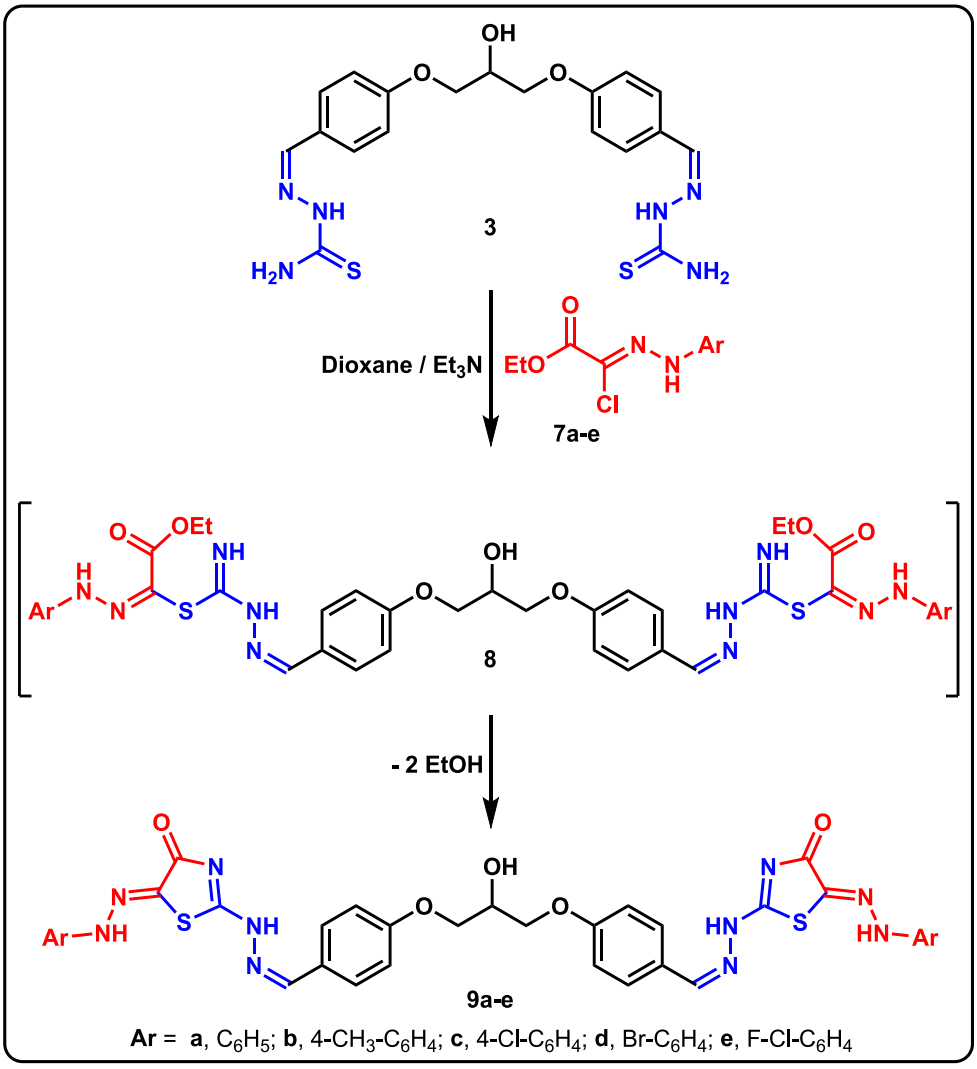

Scheme 3. Synthesis of bis-thiazole derivatives **9a-e.**

paramagnetic divalent (Co(II)) and diamagnetic divalent (Zn(II)) and they considered as biological important elements. Drawing from earlier research on the synthesis and characterization of several transition metal complexes of newly created molecules (Abd El Salam et al., 2023; Moustafa et al., 2022); metal complexes with a metal/ligand ratio of 2:1 were believed to be formed as depicted from the elemental analyses and other data (Table 1). The proposed complex structure was established based on a simple spatial arrangement that allows coordination of the chelating bis-dihydrazothiazole derivative **6a** and the corresponding metal ions (Iron(III), cobalt(II), and zinc(II)) with the least steric hindrance.

Unlike the yellowish-orange color of their parent bis-dihydrazothiazole derivative **6a**, dark, brown-colored metal chelates were formed. The color of the obtained complexes was attributed to the d → d transitions and the high effect of charge transfer which is a clear confirmation for the formation of the desired chelate complexes. Characterization of the synthesized chelate complexes was supported with elemental analyses, spectroscopic techniques, molar conductivity, magnetic moment measurements, as well as thermogravimetric analysis (TG). Based on elemental analyses data, all complexes conform to the general composition M_2L, where M=Fe(III), Co(II), or Zn(II); L=bis-dihydrazothiazole ligand **6a** (Table 1). The synthesized chelates were isolated in a powder form. The synthesized complexes were sufficiently soluble in DMF and dimethyl sulfoxide (DMSO) for molar conductivity measurements and insoluble in water, ethanol, chloroform or methanol. These complexes were found to have molar conductivity values of 16, 96, and 99 $\Omega^{-1}mol^{-1}cm^2$ for Fe(III), Co(II), and Zn(II) ions respectively (Table 1). These molar conductivity values reflect the electrolytic nature of the Co(II) and Zn(II) complexes and the non-electrolytic nature of the Fe(III) complex. Additionally, it confirmed the complexes' proposed formula, which was indicated by the elemental studies. The peaks in the ^1H NMR spectra of the Zn(II) complex corresponded to the aromatic, NH, and OH protons, and they were exactly in the same positions as those in the spectrum of the bis-dihydrazothiazole derivative 6a. Attempts to isolate single crystals for the formed complexes were unsuccessful (see experimental section).

The diffused reflectance spectrum of Co(II) complex contained three bands at 10,290 ($^4T_{1g}$ (F)→$^4T_{2g}$(F)(υ_1)), 16,559 ($^4T_{1g}$(F)→$^4A_{2g}$(F)(υ_2)), and 19,889 cm^{-1} ($^4T_{1g}$(F)→$^4T_{2g}$(P) (υ_3)) transitions. The magnetic value was found to be 4.61 BM supporting octahedral geometry (Table 1) (Moustafa et al., 2022; Kyhoiesh et al., 2021). Fe(III) complex diffused reflectance spectrum exhibited three d-d bands at 11,780 ($^6A_{1g}$(S)→$^4T_{1g}$(G) (υ_1)), 16,353 ($^6A_{2g}$(S)→$^4T_{2g}$(G) (υ_2)), and 25,350 cm^{-1} ($^6A_{1g}$(S)→$^4A_{1g}$(G) (υ_3)), transitions indicating an octahedral geometry around the Fe(III) ion, which is also supported by its magnetic moment value of 5.66 BM (Table 1) (Moustafa et al., 2022; Kyhoiesh et al., 2021). However, the diamagnetic nature of the Zn(II) complex suggested an octahedral geometry (Fig. 2). The geometry of the

Table 1
Elemental analyses, IR and thermal analysis data of metal complexes.

Elemental Analyses									
Complex	Color(% yield)	M.P (°C)	**% Found (Calcd.)**					μ_{eff}(B.M)	Λ_m $\Omega^{-1}mol^{-1}cm^2$
			C	H	N	S	M		
$[Fe_2(L)(NO_3)_6]$	Brown(84)	>300	36.51 (36.55)	2.78 (2.80)	18.27(18.44)	4.98 (5.27)	9.93 (9.22)	5.66	16
$[Co_2(L)(OAc)_2(H_2O)_4](AcO)_2{\cdot}2H_2O$	Brown(90)	>300	45.28(45.27)	4.80 (4.86)	11.58(11.74)	5.18 (5.37)	9.73 (9.89)	4.61	96
$[Zn_2(L)(OAc)_2(H_2O)_4](AcO)_2{\cdot}2H_2O$	Brown(85)	>300	44.68 (44.82)	4.80 (4.81)	11.48(11.62)	5.11 (5.31)	10.58 (10.79)	Diam	99
IR									
	ν(C=N) thiazole	ν(C=N) azomethine	ν(N=N)azo	ν(C-S)	ν(M−O)	ν(M−N)	ν(M−S)		
$[Fe_2(L)(NO_3)_6]$	1680 s	1636sh	1470 m	1050 m, 74as	510w	470 s	430 s		
$[Co_2(L)(OAc)_2(H_2O)_4](AcO)_2{\cdot}2H_2O$	1659sh	disappeared	1450 s	1026 m, 750 s	575 s	500 s	450w		
$[Zn_2(L)(OAc)_2(H_2O)_4](AcO)_2{\cdot}2H_2O$	1650 s	1630sh	1475 s	1026 m, 756 m	575w	480 s	430w		
TG									
	TG range °C	DTG_{max}, °C	Mass loss%F (%Calcd)	Total mass loss	Assignment	Residue			
$[Fe_2(L)(NO_3)_6]$	30–200	62	37.96 (38.11)	87.18 (86.76)	Loss of $6NO_3$ and C_6H_5N	Fe_2O_3			
	200–800	309, 550	49.22 (48.65)		Loss of $C_{31}H_{29}N_9S_2$				
$[Co_2(L)(OAc)_2(H_2O)_4](AcO)_2{\cdot}2H_2O$	30–250	180	33.97 (33.78)	86.71 (87.35)	Loss of $4H_2O$, 2AcO and $C_{10}H_{11}NO_2$Loss of remaining ligand	2 CoO			
	250–800	467	52.74 (53.57)						
$[Zn_2(L)(OAc)_2(H_2O)_4](AcO)_2{\cdot}2H_2O$	30–110	67	7.40 (7.89)	86.04 (86.49)	Loss of $2H_2O$ and $C_2H_3O_2$	2 ZnO			
	110–800	287, 545	78.64 (78.60)		Loss of $C_{43}H_{51}N_{10}O_{11}S_2$				

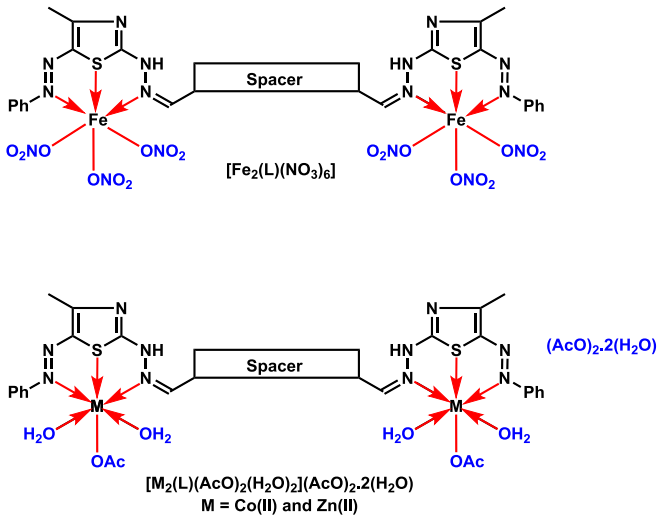

Fig. 2. Geometrical structures of the metal chelate (Fe(III), Co(II), or Zn(II)) with bis-dihydrazothiazole ligand (L).

complexes supported the elemental analyses and hence correlate with the suggested formula.

3.2.2. *Thermal analysis study*

For Fe(III), Co(II), and Zn(II)–L complexes, thermogravimetric (TG) and differential thermogravimetric (DTG) studies were performed under ambient conditions (Table 1 and Supplementary Fig. 1). The plausible complexes formula as well as correlations between the various decomposition processes of the complexes and the related weight losses are thoroughly discussed in this section.

Complex $[Fe_2(L)(NO_3)_6]$ underwent thermal decomposition over three successive steps (Supplementary Fig. 1a). The first step estimated mass loss of 37.96 % (calculated mass loss = 38.11 %) over a 30–200 °C temperature range could be attributed to the loss of $6NO_3$ and C_6H_5N fragments. The DTG curve had a peak at 62 °C (the maximum peak temperature). The second and third steps had an estimated mass loss of 49.22 % (calculated mass loss = 48.65 %) over a temperature range of 200–800 °C could be attributed to the loss of $C_{31}H_{29}N_9S_2$ fragment, leaving behind a Fe_2O_3 residue. The DTG curve had two peaks at 309 and 550 °C (the maximum peak temperature). Overall, thermal decomposition indicated a total estimated mass loss of 87.18 % (calculated mass loss = 86.76 %).

The thermal decomposition of complex $[Co_2(L)(H_2O)_4(AcO)_2].2AcO{\cdot}2H_2O$ (Supplementary Fig. 1b) underwent thermal decomposition over two main degradation steps. The first step estimated mass loss of 33.97 % (calculated mass loss = 33.78 %) over a 30–250 °C temperature range could be attributed to the loss of hydrated and coordinated water molecules, two acetates, and $C_{10}H_{11}NO_2$ fragments. The DTG curve had a maximum peak temperature of 180 °C. The second step estimated mass loss of 52.74 % (calculated mass loss = 53.57 %) over a temperature range of 250–800 °C could be attributed to the loss of the remaining portion of the ligand molecule, leaving behind a 2CoO residue. The DTG curve had an exothermic peak at 467 °C (the maximum peak temperature). Overall, thermal decomposition indicated a total estimated mass loss of 86.63 % (calculated mass loss = 87.35 %).

The thermal decomposition of complex $[Zn_2(L)(H_2O)_4(AcO)_2].2AcO{\cdot}2H_2O$ (Supplementary Fig. 1c) underwent thermal decomposition over three main degradation steps. The first step estimated mass loss of 7.40 % (calculated mass loss = 7.89 %) over a temperature range of 30–110 °C could be attributed to the liberation of two hydrate water molecules and $C_2H_3O_2$ fragments. The DTG curve had a peak at 67 °C (the maximum peak temperature). The second and third steps estimated mass loss of 78.64 % (calculated mass loss = 78.60 %) over a temperature range of 110–800 °C could be attributed to the decomposition of the remaining portion of the ligand molecule ($C_{43}H_{51}N_{10}O_{11}S_2$), leaving behind a 2ZnO residue. The DTG curve had two peaks at 287 and 545 °C (the maximum peak temperature). The overall thermal decomposition indicated a total estimated mass loss of 86.04 % (calculated mass loss = 86.49 %). The acquired results showed good correlations with the other data and elemental data.

3.2.3. IR spectral study

Examining the FT-IR spectra of the free bis-dihydrazothiazole ligand **6a** and its corresponding metal chelates M_2L; M=Fe(III), Co(II), and Zn (II); L=bis-dihydrazothiazole derivative **6a**, more insights were revealed about the molecular structure of the formed chelate complex M_2L and the coordination mechanism of the bis-dihydrazothiazole ligand (L) around the metal ion (M) (Table 1 and Supplementary Fig. 2a-c). First, the free bis-dihydrazothiazole ligand **6a** and metal complexes showed the characteristic IR absorption bands which correspond to the –OH and –NH groups at typical positions. The thiazole C=N group appeared at 1674 cm^{-1} in the bis-dihydrazothiazole ligand which shifted to lower ranges upon formation of the metal complexes at 1650–1680 cm^{-1}. The shift in the IR absorption band of the thiazole group for the metal complexes could be attributed to the skeletal bending of the bis-dihydrazothiazole ligand upon coordination with metal ions (Magaldi et al., 2004; Abd El Salam et al., 2023). Secondly, the wavenumbers of the azomethine (C=N) and the azo group (N=N) in the bis-dihydrazothiazole FT-IR spectrum revealed two peaks at 1620 and 1470 cm^{-1}, respectively, which shifted to 1630 cm^{-1} (for the Fe(III) and Zn(II) complexes and completely vanished for the Co(II) complex) and 1450–1475 cm^{-1} (Magaldi et al., 2004; Abd El Salam et al., 2023). These changes indicated the formation of bonding coordination between both the azo- group and the azomethine nitrogen in the bis-dihydrazothiazole ligand and the metal ions (Magaldi et al., 2004; Abd El Salam et al., 2023). Thirdly, the υ(C-S) band, which is present in the free bis-dihydrazothiazole ligand at 1050 and 741 cm^{-1}, was observed as two discrete bands in the FT-IR spectra of all metal complexes at 1018–1026 and 750–756 cm^{-1} (Kyhoiesh and Hassan, 2024; Kyhoiesh and Al-Adilee, 2023; Kyhoiesh and Al-Adilee, 2022). This provided additional proof that thiazole S and the metal ions were coordinated. Additionally, and as a result of this coordination process, three additional bands that corresponded to υ(M−O), υ(M−N), and υ(M−S) were observed in the FT-IR spectra of all metal complexes at 510–575 cm^{-1}, 470–500 cm^{-1}, and 430–450 cm^{-1}, respectively. (Kyhoiesh and Hassan, 2024; Kyhoiesh and Al-Adilee, 2023; Kyhoiesh and Al-Adilee, 2022).

On account of the bis-dihydrazothiazole ligand coordination to metal ions via the N, O, and S donor atoms of the characteristic bands, C-S, C=N, and N=N, respectively, and based on our previously reported researches (Magaldi et al., 2004; Abd El Salam et al., 2023); it was concluded that the bis-dihydrazothiazole ligand behaves as a neutral tridentate ligand. (Kyhoiesh and Hassan, 2024; Kyhoiesh and Al-Adilee, 2023; Kyhoiesh and Al-Adilee, 2022).

Each metal ion is surrounded by a single ligand molecule as revealed by the CHN analyses and is coordinated by three donor atoms as evidenced by the IR spectral data. A detailed summary of all metal complexes FT-IR spectra was provided in Table 1. Based on these findings, it is clear why the structure depicted in Fig. 2 is the most plausible conformation of the newly synthesized metal complexes.

3.2.4. Surface morphology

3.2.4.1. XRD study. Using X-ray diffraction patterns, the phase and crystallinity of the ligand and its complexes have been examined. The PXRD pattern of the synthesized bis-dihydrazothiazole ligand **6a** and its complexes (Supplementary Fig. 3a–d) was displayed. The large intensity peak implies that the synthesized bis-dihydrazothiazole ligand **6a** and its complexes are crystallinity. Through comparing the bis-dihydrazothiazole ligand **6a** and complex patterns, it was discovered that the most characteristic ligand peaks appeared in all synthesized complexes in addition to apparent characteristic peaks for the iron, cobalt, and zinc species, which further confirms the complexes' synthesis and the incorporation of the bis-dihydrazothiazole ligand **6a** structure into them (Orooji et al., 2020; Ghanbari and Salavati-Niasari, 2021; Karami et al., 2021).

3.2.4.2. SEM study. Material morphologies were examined using a scanning electron microscope (SEM). The free bis-dihydrazothiazole ligand **6a** and its complexes were subjected to SEM analysis as shown in Supplementary Figure 4a-d, which showed a compact, crystalline homogenous material with a porous structure. The atoms were arranged in a well-defined pattern with a smooth surface and a well-defined grain-like morphology (Orooji et al., 2020; Ghanbari and Salavati-Niasari, 2021; Karami et al., 2021).

4. Antimicrobial activity screening of the novel bis-dihydrazothiazole derivatives and three of their metal chelates with transition metal ions; Fe^{+3}, Co^{+2}, and Zn^{+2}

The antibacterial capacity of the novel hydroxy-tagged bis-dihydrazothiazole derivatives along with the three synthesized metal complexes were evaluated using the agar well diffusion method. Six microbial species were screened; two Gram-negative bacterial strains, *Salmonella typhimurium* (ATCC 14028) and *Escherichia coli* (ATCC 25955); two Gram-positive bacterial strains, *Bacillus subtilis* (NRRL B-543) and *Staphylococcus aureus* (ATCC:13565); and two fungal species, *Aspergillus fumigatus* and *Candida albicans* (ATCC:10231).

Dimethyl sulfoxide (DMSO) was used as a negative control, and ketoconazole and gentamycin were used as positive standards for bacterial and fungal species, respectively. The collected data were summarized in Table 1 and graphically represented in Fig. 3.

From the data presented in Table 2 and Graph 3A for the hydroxy-tagged bis-dihydrazothiazole derivatives **6a-e** series, the following observations could be made. Whereas compound **6c** showed excellent inhibition of *B. subtilis, E. coli*, and *C. albicans,* it showed only good inhibition of *S. coccus* and *A. fumigatus*. While compounds **6a** and **6d** showed excellent inhibition of *B. subtilis* and *E. coli*, respectively, both compounds showed only good inhibition of *C. albicans*.

From the data presented in Table 2 and graph 3B for the hydroxy-tagged bis-dihydrazothiazolone derivatives **9a-e** series, the following observations could be made. Compound **9c** showed excellent inhibition of *S. typhimurium.* However, it showed only good inhibition of *S. coccus.* While compound **9d** showed excellent inhibition of *B. subtilis,* it showed only good inhibition of both *A. fumigatus* and *C. albicans.* Whereas compound **9e** showed excellent inhibition of *S. coccus,* it showed only good inhibition of both *B. subtilis* and *E. coli.* This high antimicrobial potency of bis-dihydrazothiazole derivatives **6c** and **9c** could be attributed to an optimum charge/radius ratio of the chlorine atom.

Finally, and from the data presented in Table 2 and Graph 3. C for the metal chelates **[M_2L]** series, the following observations could be made. Complex **[Zn_2L]** showed great inhibition of both *S. coccus and S. typhimurium* compared to the reference standard *gentamycin*, and was more potent than the free ligand, **6a** itself, nonetheless. While complexes **[Fe_2L]** and **[Co_2L]** showed only good inhibition against *S. coccus* and *A. fumigatus* compared to the reference standards *gentamycin* and

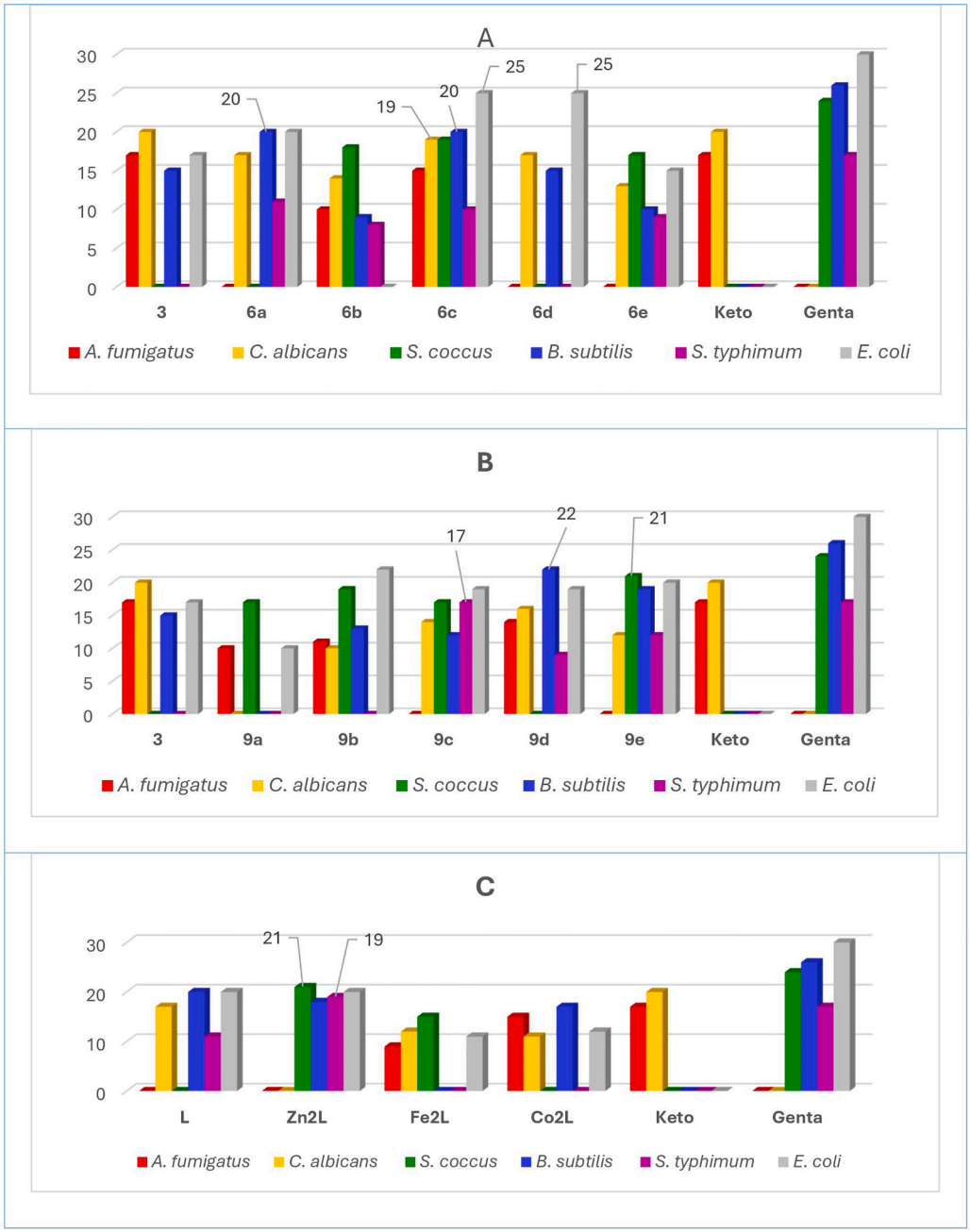

Fig. 3. Antibacterial activity of the synthesized compounds represented by the diameter of zone of inhibition (mm), **A**) Series **6a-e**, **B**) Series **9a-e**, and **C**) Metal complexes $\mathbf{M_2L}$, M=Fe, Co, Zn; L=Ligand, **6a; Keto** = ketoconazole, **Genta** = gentamycin, well diameter: 6.0 mm, sample volume: 50 µL, sample concentration: 10 µg/ml.

ketoconazole, respectively, both complexes were more potent than the free ligand, nevertheless. Whereas complex **[Co_2L]** showed only good inhibition of *A. fumigatus* compared to the reference standard *ketoconazole*, it was still more potent than the free ligand itself, nonetheless. The higher activity of the metal complexes, **[M_2L]** against six microbial species, as compared to the free ligand, could be attributed to the chelation hypothesis effect. Chelation increases the lipophilic character of the complex metal atom and helps its crossover through the microbial lipid membrane enhancing, significantly, the complex overall antimicrobial activity (Sharma et al., 2022).

It is worth mentioning that according to Mahmoud and Abass (Mahmood and Pharmaceutical, 2020); the azo-Schiff base ligand exhibited antibacterial action against Staphylococcus aureus and Escherichia coli pathogens, while its Co(II) complex remained inert. This is not the case with the results presented in this article.

5. Conclusions

The synthesis of various hydroxy-tagged bis-dihydrazothiazole derivatives **6a-e** and bis-dihydrazothiazolones derivatives **9a-e** was successfully established using a bis-thiosemicarbazone derivative **3** as a common synthetic scaffold. The chelation affinity of the novel bis-dihydrazothiazole derivatives was explored by coordinating with the metal ions; Fe(III), Co(II), or Zn(II) using **6a** as a representative bis-dihydrazothiazole ligand. It was elucidated that bis-dihydrazothiazole **6a** behaves as a neutral tridentate ligand through coordination of the

Table 2
Antibacterial activity of the synthesized compounds at 10 μm/mL.

	Diameter of zone of inhibition (mm) at 10 μm/mL					
Sample	*A. fumigatus*	*C. albicans*	*S. aureus*	*B. subtilis*	*S. typhimurium*	*E. coli*
3	38.11	44.84	NA	33.63	NA	38.11
6a	NA	23.28	NA	27.39	15.06	27.39
6b	13.19	18.46	23.74	11.87	10.55	NA
6c	18.77	23.77	23.77	25.03	12.51	31.28
6d	NA	19.14	NA	16.89	NA	28.15
6e	NA	16.97	22.19	13.05	11.74	19.58
9a	13.62	NA	23.16	NA	NA	13.62
9b	14.43	13.12	24.93	17.06	NA	28.87
9c	NA	17.43	21.17	14.94	21.17	23.66
9d	15.69	17.93	NA	24.66	10.08	21.30
9e	NA	15.58	27.27	24.67	15.58	25.97
$[Zn_2L(AcO)_2(H_2O)_4]2AcO{\cdot}2H_2O$	NA	NA	18.98	16.27	17.17	18.08
$[Fe_2L(NO_3)_6]$	7.77	10.36	12.95	NA	NA	9.49
$[Co_2L(AcO)_2(H_2O)_4]2AcO{\cdot}2H_2O]$	14.47	10.61	NA	16.40	NA	11.58
Ketoconazole	32.01	37.66	–	–	–	–
Gentamycin	–	–	50.31	54.50	35.63	62.89
DMSO	0.0	0.0	0.0	0.0	0.0	0.0

Negative control is DMSO. Positive control for fungal species (ketoconazole, 100 μg/disc) and positive control for both Gram-negative bacteria and Gram-positive bacteria (gentamycin, 4 μg/disc), *NA: No activity.

azomethine-*N*, thiazole-*S*, and azo-*N* atoms forming octahedral metal complexes with a metal/ligand ratio of 2:1. Both Co(II) and Zn(II) complexes were electrolytes. However, Fe(III) complex was nonelectrolyte. All complexes displayed two to three breakdown phases within the temperature range of 30–800 °o., as inferred from the TG data, they showed two to three decomposition steps within the temperature range 30–800 °C as concluded from TG results. The XRD investigation showed that the bis-dihydrazothiazole derivative **6a** and its metal chelates were crystalline in nature. The antimicrobial capacities of the novel hydroxy-tagged bis-dihydrazothiazole derivatives **6a-e** and **9a-e**, as well as some of their metal chelates with (Fe(III), Co(II), or Zn(II) were conducted against six different microbes using ketoconazole and gentamycin as antimicrobial reference standards utilizing the agar well diffusion method. Most compounds showed decent to excellent antimicrobial activities against the screened microbes. However, the chloro-substituted bis-dihydrazothiazole derivatives **6c** and **9c** showed exceptional reactivities. Compound **6c** showed excellent inhibition of *B. subtilis* (20 mm), *E. coli* (25 mm), and *C. albicans* (17 mm), while compounds **9c** showed excellent inhibition of *S. typhimurium* (17 mm) and *E. coli* (19 mm), respectively. This high antimicrobial potency of bis-dihydrazothiazole derivatives **6c** and **9c** could be endorsed by an optimum charge/radius ratio of the chlorine atom. On the other hand, amongst the three synthesized metal complexes, only the [Zn(II) complex showed remarkable inhibition of both *S. aureus* (21 mm), *S. typhimurium* (20 mm), and *E. coli* (20 mm) compared to the reference standard gentamycin.

It was significantly more potent than the free ligand, **6a** itself. This improved reactivity could be attributed to increased lipophilicity of the complex metal atom which, sequentially, helps its crossover through the microbial lipid membrane enhancing, significantly, the complex overall antimicrobial activity compared to the free ligand itself. On another note, both Fe(III) and Co(II) complexes showed decent antifungal activity against *A. fumigatus*, 9 and 15 mm, respectively.

Further functionalization of the free –OH group and extensive investigation of the biological spectrum of the new hydroxy-tagged bis-dihydrazothiazole derivative, and its metal complexes are currently underway.

CRediT authorship contribution statement

Refaie M. Kassab: Writing – review & editing, Writing – original draft, Visualization, Validation, Supervision, Software, Resources, Project administration, Methodology, Investigation, Funding acquisition, Formal analysis, Data curation, Conceptualization. **Sami A. Al-Hussain:** Writing – review & editing, Project administration, Funding acquisition. **Magdi E.A. Zaki:** Writing – review & editing, Supervision, Funding acquisition, Conceptualization. **Gehad G. Mohamed:** Writing – original draft, Resources, Formal analysis, Data curation. **Zeinab A. Muhammad:** Writing – review & editing, Writing – original draft, Software, Resources, Project administration, Methodology, Formal analysis, Data curation.

Declaration of Competing Interest

The authors declare that they have no known competing financial interests or personal relationships that could have appeared to influence the work reported in this paper.

Acknowledgment

This work was supported and funded by the Deanship of Scientific Research at Imam Mohammad Ibn Saud Islamic University (IMSIU) (grand number IMSIU-RP23080).

Appendix A. Supplementary data

Supplementary data to this article can be found online at https://doi.org/10.1016/j.arabjc.2024.105933.

References

Abd El Salam, H.A., Moustafa, G., Zayed, E.M., Mohamed, G.G., 2023. Isophthaloylbis (Azanediyl) Dipeptide Ligand and Its Complexes: Structural Study, Spectroscopic, Molecular Orbital, Molecular Docking, and Biological Activity Properties. Available from: Polycycl. Aromat. Compd. [Internet] 43 (6), 4866–4888 https://www.tandfonline.com/doi/abs/10.1080/10406638.2022.2097712.

Abdelhamid, A.O., Shawali, A.S., Gomha, S.M., El-Enany, W.A.M.A., 2015. Synthesis and antimicrobial evaluation of some novel thiazole, 1,3,4-thiadiazole and pyrido[2,3-D][1,2,4]- TRIAZOLO[4,3-A]pyrimidine derivatives incorporating pyrazole moiety. Heterocycles. 91 (11), 2126–2142.

Abdel-Wahab, B.F., Mohamed, S.F., Amr, A.E.G.E., Abdalla, M.M., 2008. Synthesis and reactions of thiosemicarbazides, triazoles, and Schiff bases as antihypertensive α-blocking agents. Monatshefte Fur Chemie. 139 (9), 1083–1090.

Al-Hussain, S.A., Farghaly, T.A., Ibrahim, M.H., et al., 2024. The anti-breast cancer activity of indeno[1,2-b]pyridin-5-one and their hydrazonal precursors endowed with anti-CDK-2 enzyme activity. J. Mol. Struct. 1295, 136692.

Borcea, A.M., Ionuț, I., Crișan, O., Oniga, O., 2021. An overview of the synthesis and antimicrobial, antiprotozoal, and antitumor activity of thiazole and bisthiazole derivatives. Available from Molecules [internet] 26 (3), 624. https://www.mdpi.com/1420-3049/26/3/624/htm.

Cascioferro, S., Parrino, B., Carbone, D., et al., 2020. Thiazoles, Their Benzofused Systems, and Thiazolidinone Derivatives: Versatile and Promising Tools to Combat Antibiotic Resistance. Available from: J. Med. Chem. [Internet] 63 (15), 7923–7956 https://pubs.acs.org/doi/full/10.1021/acs.jmedchem.9b01245.

Clough, J.M., Dube, H., Martin, B.J., Pattenden, G., Reddy, K.S., Waldron, I.R., 2006. Total synthesis of myxothiazols, novel bis-thiazole β-methoxyacrylate- based antifungal compounds from myxobacteria. Available from: Org. Biomol. Chem. [Internet] 4 (15), 2906–2911 https://pubs.rsc.org/en/content/articlehtml/2006/ob/b603433k.

Dawood, K.M., Gomha, S.M., 2015. Synthesis and Anti-cancer Activity of 1,3,4-Thiadiazole and 1,3-Thiazole Derivatives Having 1,3,4-Oxadiazole Moiety. J. Heterocycl. Chem. 52 (5), 1400–1405.

Franklin, P.X., Pillai, A.D., Rathod, P.D., et al., 2008. 2-Amino-5-thiazolyl motif: A novel scaffold for designing anti-inflammatory agents of diverse structures. Eur. J. Med. Chem. 43 (1), 129–134.

Ghanbari, M., Salavati-Niasari, M., 2021. Copper iodide decorated graphitic carbon nitride sheets with enhanced visible-light response for photocatalytic organic pollutant removal and antibacterial activities. Ecotoxicol. Environ. Saf. 208, 111712.

Gomha, S., Khalil, K., Abdel-Aziz, H., Abdalla, M., 2015. Synthesis and anti-hypertensive ?-blocking activity evaluation of thiazole derivatives bearing pyrazole moiety. Heterocycles. 91 (9), 1763–1773.

Israr, A., Hameed, S., Al-Masoudi, N.A., 2024. Synthesis, anti-HIV and cytotoxicity evaluation of chiral 2,5-disubstituted 1,3,4-Thiadiazole derivatives bearing the sulfonamide scaffold.. Available from: Zeitschrift Fur Naturforsch. - Sect. B J. Chem. Sci. [internet] 79 (2–3), 89–97 https://www.degruyter.com/document/doi/10.1515/znb-2023-0078/html.

Karami, M., Ghanbari, M., Alshamsi, H.A., Rashki, S., Salavati-Niasari, M., 2021. Facile fabrication of Tl4HgI6nanostructures as novel antibacterial and antibiofilm agents and photocatalysts in the degradation of organic pollutants. Available from: Inorg. Chem. Front. [Internet] 8 (10), 2442–2460 https://pubs.rsc.org/en/content/articlehtml/2021/qi/d1qi00155h.

Karges, J., Stokes, R.W., Cohen, S.M., 2021. Metal complexes for therapeutic applications. Available from: Trends Chem. [Internet]. 3 (7), 523–534 http://www.cell.com/article/S2589597421000605/fulltext.

Kassab, R.M., Elwahy, A.H.M., Abdelhamid, I.A., 2016. 1, ω-Bis(formylphenoxy)alkane: versatile precursors for novel bis-dihydropyridine derivatives. Monatshefte Fur Chemie. 147 (7), 1227–1232.

Kassab RM, Gomha SM, Al-Hussain SA, *et al.* Synthesis and In-silico Simulation of Some New Bis-thiazole Derivatives and Their Preliminary Antimicrobial Profile: Investigation of Hydrazonoyl Chloride Addition to Hydroxy-Functionalized Bis-carbazones. *Arab. J. Chem.* [Internet]. 14(11), 6 (2021). Available from: https://www.sciencedirect.com/science/article/pii/S1878535221004111.

Kassab RM, A Zaki ME, Abo Dena AS, Al-Hussain SA, Abdel-Aziz MM, Muhammad ZA. Novel Set of Highly Substituted Bis-pyridines: Synthesis, Molecular Docking and Drug-Resistant Antibacterial Profile. *Future Med. Chem.* [Internet]. 14(24), 1881–1897 (2022). Available from: https://www.future-science.com/doi/10.4155/fmc-2022-0196.

Kassab RM, Zaki MEA, Al-Hussain SA, Abdelmonsef AH, Muhammad ZA. Two Novel Regioisomeric Series of Bis-pyrazolines: Synthesis, In Silico Study, DFT Calculations, and Comparative Antibacterial Potency Profile against Drug-Resistant Bacteria; MSSA, MRSA, and VRSA. *ACS Omega* [Internet]. (2023). Available from: https://pubs.acs.org/doi/full/10.1021/acsomega.3c06348.

Kassab, R.M., Gomha, S.M., Muhammad, Z.A., Synthesis, E.-K., 2020. Biological Profile, and Molecular Docking of Some New Bis- Imidazole Fused Templates and Investigation of their Cytotoxic Potential as Anti-tubercular and/or Anticancer Prototypes. Med. Chem. (los. Angeles). 17 (8), 875–886.

Kassab, R.M., Al-Hussain, S.A., Elleboudy, N.S., et al., 2022. Tackling Microbial Resistance with Isatin-Decorated Thiazole Derivatives: Design, Synthesis, and in vitro Evaluation of Antimicrobial and Antibiofilm Activity. Available from: Drug Des. Devel. Ther. [Internet] 16, 2817–2832 https://pubmed.ncbi.nlm.nih.gov/36046334/.

Kassab, R.M., Khalil, F.S.A.M., Abbas, A.A., 2022. Synthesis and Antimicrobial Activities of Some New Bis(Schiff Bases) and Their Triazole-Based Lariat Macrocycles. Polycycl. Aromat. Compd. 42 (5), 2751–2766.

Kassab, R.M., Muhammad, Z.A., Al-Hussain, S.A., et al., 2023. Indeno[1,2-b]pyridin-5-one derivatives containing azo groups and their hydrazonal precursors: Synthesis, antimicrobial profile, DNA gyrase binding affinity, and molecular docking. Available from: J. Heterocycl. Chem. [Internet] https://onlinelibrary.wiley.com/doi/full/10.1002/jhet.4759.

Kassab, R.M., Al-Hussain, S.A., Abdelmonsef, A.H., Zaki, M.E.A., Gomha, S.M., Muhammad, Z.A., 2024. Novel xylenyl-spaced bis-thiazoles/thiazines: synthesis, biological profile as herpes simplex virus type 1 inhibitors and in silico simulations. Available from: Future Med. Chem. [Internet] 16 (1), 27–41 https://www.future-science.com/doi/10.4155/fmc-2023-0210.

kassab RM, Ibrahim MH, Rushdi A, *et al.* Comprehensive study for synthesis, antiviral activity, docking and ADME study for the new fluorinated hydrazonal and indeno [1,2-b]pyridine derivatives. *J. Mol. Struct.* [Internet]. 1305, 137752 (2024). Available from: https://linkinghub.elsevier.com/retrieve/pii/S0022286024002758.

Kouatly, O., Geronikaki, A., Kamoutsis, C., Hadjipavlou-Litina, D., Eleftheriou, P., 2009. Adamantane derivatives of thiazolyl-N-substituted amide, as possible non-steroidal anti-inflammatory agents. Eur. J. Med. Chem. 44 (3), 1198–1204.

Kyhoiesh, H.A.K., Al-Adilee, K.J., 2023. Pt(IV) and Au(III) complexes with tridentate-benzothiazole based ligand: synthesis, characterization, biological applications (antibacterial, antifungal, antioxidant, anticancer and molecular docking) and DFT calculation. Inorganica Chim. Acta. 555, 121598.

Kyhoiesh, H.A.K., Al-Hussainawy, M.K., Waheeb, A.S., Al-Adilee, K.J., 2021. Synthesis, spectral characterization, lethal dose (LD50) and acute toxicity studies of 1,4-Bis (imidazolylazo)benzene (BIAB). Heliyon. 7 (9).

Kyhoiesh HAK, Al-Adilee KJ. Synthesis, spectral characterization and biological activities of Ag(I), Pt(IV) and Au(III) complexes with novel azo dye ligand (N, N, O) derived from 2-amino-6-methoxy benzothiazole. *Chem. Pap.* [Internet]. 76(5), 2777–2810 (2022). Available from: https://link.springer.com/article/10.1007/s11696-022-02072-9.

Kyhoiesh, H.A.K., Hassan, H.M., 2024. Synthesis, Characterization, in silico DFT, Molecular docking, ADMET Profiling Studies and Toxicity Predictions of Ag(I) Complex Derived from 4-Aminoacetophenone. Available from ChemistrySelect [Internet] 9 (4), e202304429. https://onlinelibrary.wiley.com/doi/full/10.1002/slct.202304429.

Limban, C., Chifiriuc, M.C.B., Missir, A.V., Chiriţă, I.C., Bleotu, C., 2008. Antimicrobial activity of some new thioureides derived from 2-(4-chlorophenoxymethyl)benzoic acid. Molecules. 13 (3), 567–580.

Magaldi, S., Mata-Essayag, S., Hartung De Capriles, C., et al., 2004. Well diffusion for antifungal susceptibility testing. Int. J. Infect. Dis. 8 (1), 39–45.

Mahmood R, Pharmaceutical HA-IJ of, 2020 undefined. Synthesis, Characterization and Biological Activities of Azo and Azomethine Ligand with Some Transition Metal Complexes. *Res. Mahmood, H AbassInternational J. Pharm. Res. 2020•researchgate.net* [Internet]. 12(2), 258–263 (2020). Available from: https://www.researchgate.net/profile/Rasha-Mahmood/publication/348906855_Synthesis_Characterization_and_Biological_Activities_of_Azo_and_Azomethine_Ligand_with_Some_Transition_Metal_Complexes/links/60155a9945851517ef273a28/Synthesis-Characterization-and-Biological-Activities-of-Azo-and-Azomethine-Ligand-with-Some-Transition-Metal-Complexes.pdf.

Mahmoud, H.K., Kassab, R.M., Gomha, S.M., 2019. Synthesis and characterization of some novel bis-thiazoles. Available from: *J. Heterocycl. Chem.* [internet]. 56 (11), 3157–3163 https://onlinelibrary.wiley.com/doi/full/10.1002/jhet.3717.

Moustafa, G., Sabry, E., Zayed, E.M., Mohamed, G.G., 2022. Structural characterization, spectroscopic studies, and molecular docking studies on metal complexes of new hexadentate cyclic peptide ligand. Available from: Appl. Organomet. Chem. [Internet] 36 (2), e6515 https://onlinelibrary.wiley.com/doi/full/10.1002/aoc.6515.

Niu, Z.X., Wang, Y.T., Zhang, S.N., et al., 2023. Application and synthesis of thiazole ring in clinically approved drugs. Eur. J. Med. Chem. 250, 115172.

Oka, Y., Yabuuchi, T., Fujii, Y., et al., 2012. Discovery and optimization of a series of 2-aminothiazole-oxazoles as potent phosphoinositide 3-kinase γ inhibitors. Bioorganic Med. Chem. Lett. 22 (24), 7534–7538.

Orooji, Y., Ghanbari, M., Amiri, O., Salavati-Niasari, M., 2020. Facile fabrication of silver iodide/graphitic carbon nitride nanocomposites by notable photo-catalytic performance through sunlight and antimicrobial activity. J. Hazard. Mater. 389, 122079.

Ou, M., Zhu, C., Zhang, Q.L., Zhu, B.X., 2013. Synthesis and characterization of macrocyclic compounds with a hydroxyl functional group. Chinese Chem. Lett. 24 (10), 869–872.

Petrou A, Fesatidou M, Geronikaki A. Thiazole ring—a biologically active scaffold. *Molecules* [Internet]. 26(11), 3166 (2021). Available from: https://www.mdpi.com/1420-3049/26/11/3166/htm.

Potewar, T.M., Ingale, S.A., Srinivasan, K.V., 2007. Efficient synthesis of 2,4-disubstituted thiazoles using ionic liquid under ambient conditions: a practical approach towards the synthesis of Fanetizole. Tetrahedron. 63 (45), 11066–11069.

Rajanarendar, E., Ramakrishna, S., Rama, M.K., 2012. Synthesis of novel isoxazolyl bis-thiazolo[3,2-a]pyrimidines. Chinese Chem. Lett. 23 (8), 899–902.

Rana, R., Kumar, N., Gulati, H.K., et al., 2023. A comprehensive review on thiazole based conjugates as anti-cancer agents. J. Mol. Struct. 1292, 136194.

Sanad, S.M.H., Kassab, R.M., Abdelhamid, I.A., Elwahy, A.H.M., 2016. Microwave assisted multi-component synthesis of novel bis(1,4-dihydropyridines) based arenes or heteroarenes. Heterocycles. 92 (5), 910–924.

Sayed, A.R., Gomha, S.M., Taher, E.A., et al., 2020. One-pot synthesis of novel thiazoles as potential anti-cancer agents. Drug Des. Devel. Ther. 14, 1363–1375.

Sharma, B., Shukla, S., Rattan, R., et al., 2022. Antimicrobial Agents Based on Metal Complexes: Present Situation and Future Prospects. Int. J. Biomater. 2022.

Verma, A., Saraf, S.K., 2008. 4-Thiazolidinone - A biologically active scaffold. Eur. J. Med. Chem. 43 (5), 897–905.

Watanabe, M., Uesugi, M., 2013. Small-molecule inhibitors of SREBP activation-potential for new treatment of metabolic disorders. Medchemcomm. 4 (11), 1422–1433.

Yücel, N.T., Asfour, A.A.R., Evren, A.E., et al., 2024. Design and synthesis of novel dithiazole carboxylic acid Derivatives: In vivo and in silico investigation of their Anti-Inflammatory and analgesic effects. Bioorg. Chem. 144, 107120.

Zhang, T., Yuan, C., Zhou, Q., et al., 2023. Chalcone derivatives containing thiazole fragment: Synthesis and antifungal activity. J. Saudi Chem. Soc. 27 (6), 101773.

Zhao, B., Wu, Y.J., Tao, J.C., Yuan, H.Z., Mao, X.A., 1996. Studies on the syntheses of hydroxy-bearing benzo-azacrown ethers and their complexing behaviour. Polyhedron. 15 (7), 1197–1202.